Title
A Single Set of Interneurons Drives Opposite Behaviors in C. elegans

Journal
Current Biology, 27(17)

ISSN
0960-9822

Authors
Guillermin, Manon L
Carrillo, Mayra A
Hallem, Elissa A

Publication Date
2017-09-01

DOI
10.1016/j.cub.2017.07.023

Peer reviewed

HHS Public Access

Author manuscript

Curr Biol. Author manuscript; available in PMC 2018 October 18.

Published in final edited form as:

Curr Biol. 2017 September 11; 27(17): 2630–2639.e6. doi:10.1016/j.cub.2017.07.023.

A single set of interneurons drives opposite behaviors in *C. elegans*

Manon L. Guillermin, **Mayra A. Carrillo**, and **Elissa A. Hallem***

Department of Microbiology, Immunology, and Molecular Genetics, University of California, Los Angeles, Los Angeles, CA 90095, USA

Summary

Many chemosensory stimuli evoke innate behavioral responses that can be either appetitive or aversive depending on an animal's age, prior experience, nutritional status, and environment [1–9]. However, the circuit mechanisms that enable these valence changes are poorly understood. Here, we show that *Caenorhabditis elegans* can alternate between attractive or aversive responses to carbon dioxide (CO_2) depending on its recently experienced CO_2 environment. Both responses are mediated by a single pathway of interneurons. The CO_2-evoked activity of these interneurons is subject to extreme experience-dependent modulation, enabling them to drive opposite behavioral responses to CO_2. Other interneurons in the circuit regulate behavioral sensitivity to CO_2 independent of valence. A combinatorial code of neuropeptides acts on the circuit to regulate both valence and sensitivity. Chemosensory valence-encoding interneurons exist across phyla, and valence is typically determined by whether appetitive or aversive interneuron populations are activated. Our results reveal an alternative mechanism of valence determination in which the same interneurons contribute to both attractive and aversive responses through modulation of sensory neuron to interneuron synapses. This circuit design represents a previously unrecognized mechanism for generating rapid changes in innate chemosensory valence.

Keywords

C. elegans; sensory valence; carbon dioxide response; experience-dependent modulation; olfactory behavior; gas sensing; neuromodulation; chemosensation

Results and Discussion

Here we investigated the molecular, cellular, and circuit mechanisms that determine CO_2 response in the free-living roundworm *C. elegans*. CO_2 is a byproduct of cellular respiration that can signal the presence of food, mates, predators, or pathogens [10–13]. We found that CO_2 can be attractive or repulsive for *C. elegans* adults depending on their recently experienced environmental CO_2 levels. We raised animals at either ambient or high (2.5%) CO_2 for one generation, and tested their response to CO_2 in a chemotaxis assay (Figure

*Corresponding author and lead author: ehallem@ucla.edu.

Author Contributions

Conceptualization, M.L.G., M.A.C., and E.A.H.; methodology, M.L.G., M.A.C., and E.A.H.; investigation, M.L.G. and M.A.C.; writing, M.L.G. and E.A.H.; funding acquisition, E.A.H.

S1A). Although the level of atmospheric CO_2 is only 0.038% [10], wild *C. elegans* inhabit environments rich in rotting organic matter, where CO_2 levels can rise above 10% [14]. As previously reported, animals raised at ambient CO_2 avoided CO_2 (Figure 1A) [15, 16]. In contrast, animals raised at high CO_2 showed robust CO_2 attraction (Figure 1A). In both cases, response valence was consistent across concentrations (Figure S1B–C). Thus, *C. elegans* can show attraction or repulsion to CO_2 depending on its prior cultivation conditions.

We then examined the behavior of animals raised at either ambient or 2.5% CO_2 in three different CO_2 gradients: 0–2.5%, 2.5–10%, or 2.5–40%. We found that animals raised at ambient CO_2 avoided the higher concentration of CO_2 under all three conditions (Figure S1D). By contrast, animals raised at 2.5% CO_2 were attracted to the higher CO_2 concentration in both the 0–2.5% and 2.5–10% CO_2 gradients (Figure S1D). Thus, cultivating animals at high CO_2 results in a drive toward higher CO_2 levels rather than a preference for their previous cultivation condition. This is in contrast to other sensory behaviors in *C. elegans*, including salt chemotaxis and thermotaxis, where animals are attracted to their prior cultivation condition [17, 18]. Animals raised at high CO_2 were not attracted to 40% CO_2 in the 2.5%−40% CO_2 gradient (Figure S1D), suggesting that they retain the ability to avoid toxic levels of CO_2 [19].

To determine if CO_2 preferences are flexible, we transferred animals raised at ambient CO_2 to high CO_2 and vice versa, and assayed their responses to 2.5% CO_2 over the course of 9 hours. We found that animals displayed rapid adaptation to their new environment. Animals raised at ambient CO_2 showed CO_2 attraction after 1 hour at high CO_2 and exhibited maximum attraction by 6 hours (Figure 1B). Animals raised at high CO_2 displayed decreased attraction after 3 hours at ambient CO_2 and recovery of CO_2 avoidance by 9 hours (Figure 1B). Thus, CO_2 response valence is experience-dependent and flexible.

The same pair of sensory neurons is required for CO_2 attraction and repulsion

We next investigated the mechanisms that drive CO_2-evoked behaviors of opposing valence. We previously showed that the BAG sensory neurons detect CO_2 and are required for CO_2 avoidance [12, 15, 20]. We therefore examined the role of BAG in mediating CO_2 attraction. We found that BAG is required for CO_2 attraction as well as repulsion: animals lacking BAG failed to respond to CO_2 regardless of their prior cultivation conditions (Figures 1C, S1E). We tested animals with increased neurotransmission in BAG due to cell-specific expression of a gain-of-function *(gf)* allele of the protein kinase C gene *pkc-1* [21, 22], and found that *BAG::pkc-1(gf)* animals raised at ambient CO_2 showed enhanced CO_2 avoidance (Figure S1E). Thus, BAG activity modulates the strength of the behavioral response to CO_2.

To test whether recently experienced CO_2 levels affect the response of BAG to CO_2, we compared the CO_2-evoked activity of BAG in animals raised at ambient vs. high CO_2 using calcium imaging. In animals raised at ambient CO_2, exposure to CO_2 resulted in a rapid depolarization, consistent with previous reports (Figure 1D) [12, 20, 23]. In animals raised at high CO_2, exposure to CO_2 resulted in a 2.5-fold increase in the magnitude of the depolarization (Figure 1D). In addition, the CO_2-evoked responses of BAG in animals raised at ambient CO_2 were previously shown to be concentration-dependent [20], and we observed

that the CO_2-evoked responses of BAG in animals raised at high CO_2 are also concentration-dependent (Figure S1F). Since CO_2 response valence is consistent across concentrations in animals raised at ambient or high CO_2 (Figure S1B C), yet the CO_2-evoked activity of BAG is concentration-dependent in both cases, CO_2 response valence is encoded downstream of the calcium response of BAG.

The increased BAG activity in animals raised at high CO_2 correlated with increased expression of the receptor guanylate cyclase gene *gcy-9*, which encodes a putative CO_2 receptor [20, 23–25] (Figure S2A). These results are consistent with the increased behavioral sensitivity to CO_2 exhibited by animals raised at high CO_2: whereas animals raised at ambient CO_2 are repelled by CO_2 concentrations above 5%, animals raised at high CO_2 are attracted to CO_2 concentrations as low as 0.25% (Figure S1B–C). Thus, cultivation at high CO_2 alters both the valence and sensitivity of CO_2-evoked behavior. The increased CO_2 sensitivity following prolonged exposure to high CO_2 is unusual in that prolonged exposure to a chemosensory stimulus generally results in reduced sensitivity as a result of adaptation [26], and in fact prolonged exposure of insects and fish to high CO_2 environments results in reduced sensitivity to CO_2 [27, 28]. *C. elegans* responds differently to prolonged CO_2 exposure, perhaps because it often inhabits high CO_2 environments. That the sensitivity of *C. elegans* to CO_2 may be determined by regulating the level of expression of the CO_2 receptor in BAG rather than by regulating interneuron input to BAG may reflect the fact that *C. elegans* chemosensory neurons respond to multiple chemosensory stimuli due to the compact nature of the *C. elegans* nervous system [29]. In particular, BAG responds to both CO_2 and O_2 [30], and therefore regulating the sensitivity of BAG to CO_2 by regulating CO_2 receptor expression may be a mechanism that adjusts CO_2 sensitivity while leaving O_2 sensitivity unaltered.

CO_2 avoidance and attraction require neuropeptide and glutamate signaling

We then investigated the signaling mechanisms used by BAG in animals raised at ambient vs. high CO2 to generate attractive or repulsive responses to CO_2. The FMRFamide-like neuropeptide FLP-17 is expressed specifically in BAG [31, 32]. We found that *flp-17* mutants raised at ambient CO_2 did not respond to any concentration of CO_2 (Figures 1E, S2B). By contrast, *flp-17* mutants raised at high CO_2 were still attracted to CO_2, but to a lesser extent than wild-type animals (Figures 1F, S2C). Thus, FLP-17 is required for CO_2 avoidance but acts in combination with other signaling mechanisms to mediate CO_2 attraction. A candidate for such an additional signaling mechanism is glutamate, since BAG expresses the vesicular glutamate transporter EAT-4 [33]. We found that *eat-4* mutants raised at ambient CO_2 failed to respond to CO_2, while *eat-4* mutants raised at high CO_2 showed decreased CO_2 attraction (Figures 1E–F, S2B–C). However, *eat-4; flp-17* double mutants raised at high CO_2 did not respond to CO_2, suggesting that FLP-17 and glutamate act partially redundantly to mediate CO_2 attraction (Figures 1F, S2C). Moreover, restoring *eat-4* expression specifically in BAG partially restored CO_2 avoidance and attraction (Figure S2D–E). Thus, *eat-4* acts in BAG to mediate CO_2 response, although glutamatergic signaling from other neurons may also contribute. These results indicate that BAG mediates both CO_2 avoidance and attraction via neuropeptide and glutamate signaling.

A single pathway of interneurons drives CO_2 avoidance and attraction

To gain insight into the CO_2 circuit that operates downstream of BAG, we examined the requirement for the 8 interneurons postsynaptic to BAG [34, 35] that have been previously implicated in chemosensory behaviors [36–42] (Figure S3A). We first tested whether these interneurons are required for CO_2 avoidance in animals raised at ambient CO_2 using strains in which individual interneurons or subsets of interneurons were genetically ablated or silenced with tetanus toxin [43, 44]. When tested with 1% CO_2, a concentration that is neutral to wild-type animals, AIB- AIZ- and AIY- animals showed avoidance and RIA- animals showed attraction (Figure 2A). AIB- animals responded normally to CO_2, suggesting that the phenotype of the AIBAIZ- animals resulted from the loss of AIZ activity (Figure 2A). When tested with 10% CO_2, RIG-animals showed reduced avoidance relative to wild-type animals (Figure 2B). The increased avoidance of AIB- AIZ- and AIY- animals, and the reduced avoidance of RIG- and RIA- animals, were consistent across concentrations (Figure 2C–F). In contrast, *AIY::pkc-1(gf)* animals showed weaker avoidance, while *RIG::pkc-1(gf)* and *RIA::pkc-1(gf)* animals showed enhanced avoidance relative to wild-type animals (Figure 2C–E). Transiently silencing AIY and RIA in adult animals using the histamine-gated chloride channel HisClI [45, 46] had the same effect on CÜ2-evoked behavior as genetic ablation (Figure 2G). Together, these results suggest that CO_2 avoidance is mediated by four pairs of first-order interneurons - AIY, AIZ, RIA, and RIG - whose real-time activity levels determine behavior.

To identify interneurons that regulate CO_2 attraction, we raised interneuron-ablated or silenced strains at high CO_2 and assayed their responses to 0.1% and 0.25% CO_2. Animals raised at high CO_2 were tested with lower concentrations of CO_2 than animals raised at ambient CO_2 due to their increased CO_2 sensitivity; 0.1% and 0.25% CO_2 were chosen because they elicited nonsaturating responses from wild-type animals (Figure S1C). We found that AIB- AIZ- and RIA-animals showed stronger attraction, and AIY- animals showed weaker attraction, than wild-type animals (Figure 3A–E). AIB- animals showed normal CO_2 attraction, suggesting the phenotype of AIB- AIZ- animals is due to the loss of AIZ activity (Figure 3A–B). In contrast, *AIY::pkc-1(gf)* animals raised at high CO_2 showed stronger attraction, while *RIA::pkc-1(gf)* showed weaker attraction relative to wild-type animals (Figure 3C–D). Transiently silencing AIY and RIA in animals raised at high CO_2 had the same effect on CO_2-evoked behavior as genetic ablation (Figure 3F–G). Moreover, we found that RIG- animals showed a delayed shift from attraction to avoidance following a transition from high to ambient CO_2 (Figure 3H–I). Whereas wild-type animals recovered 77% of their maximum avoidance after 6 hours, RIG- animals recovered only 11%. Conversely, AIY- animals showed a delayed shift, and RIA- animals showed an accelerated shift, from repulsion to attraction following a transition from ambient to high CO_2 (Figure 3J–K). After 3 hours at high CO_2, wild-type animals reached 81% of their maximum attraction, whereas AIY-animals reached only 23% and RIA- animals reached 99%. Taken together, these results suggest that the same set of interneurons regulates CO_2 attraction and repulsion.

AIY expresses the inhibitory glutamate-gated chloride channel subunit GLC-3 [47]. We therefore tested whether GLC-3 plays a role in suppressing AIY activity to promote CO_2

avoidance. We found that *glc-3* mutants grown at ambient CO_2 responded normally to CO_2, but *glc-3* mutants raised at high CO_2 and transferred to ambient CO_2 showed a delayed shift from attraction to repulsion (Figure S3B–C). This phenotype was rescued by cell-specific expression of *glc-3* in AIY (Figure S3C). Thus, inhibition of AIY via *glc-3* is required for animals to adapt normally to a shift from high to ambient CO_2.

We next examined the CO2-evoked activity of AIY, RIA and RIG by calcium imaging to determine how CO_2 response valence arises from the activity of these interneurons. We found that AIY showed a CO_2-evoked depolarization in animals raised at high CO_2, and a small but significant hyperpolarization in animals raised at ambient CO_2 (Figure 4A). In contrast, RIA showed a CO_2-evoked depolarization in animals raised at ambient CO_2, consistent with a previous report [48], and a CO_2-evoked hyperpolarization in animals raised at high CO_2 (Figure 4B). RIG also showed a CO2-evoked depolarization in animals raised at ambient CO2, but showed no response in animals raised at high CO_2 (Figure 4C). The CO_2-evoked responses of AIY, RIA, and RIG were BAG-dependent (Figure 4A–C). Thus, AIY, RIA, and RIG show qualitative differences in their CO_2-evoked activity in animals raised at ambient vs. high CO_2.

Together, our behavioral and calcium imaging data demonstrate that CO_2 repulsion and attraction are mediated by the coordinated activity of the same set of first-order interneurons. The CO_2-evoked activity of these interneurons is contextually modulated to drive opposite responses to CO_2. Inhibition of AIY promotes avoidance, while activation of AIY promotes attraction. In contrast, inhibition of RIA and silencing of RIG promotes attraction, while activation of RIA and RIG promotes avoidance. Thus, CO_2 avoidance arises from activation of RIA and RIG, and inhibition of AIY; CO_2 attraction arises from activation of AIY, inhibition of RIA, and silencing of RIG.

Distinct interneurons regulate valence and sensitivity

In contrast to AIY, RIA, and RIG, AIZ showed similar CO_2-evoked activity in animals raised at ambient vs. high CO_2 (Figure 4D). This activity was decreased but not eliminated in BAG- animals, suggesting additional CO2-dependent inputs into AIZ (Figure 4D). The magnitude of the depolarization in AIZ did not differ under ambient vs. high CO_2 conditions despite BAG activity being significantly different (Figures 1D, 4D), suggesting that AIZ activity may be constrained by gain control mechanisms. In addition, the fact that AIZ activity does not differ in animals raised at ambient vs. high CO_2 demonstrates that raising animals at high CO_2 does not result in a general physiological change that alters the CO_2-evoked activity of all interneurons in the circuit; rather, it results in cell-specific changes to the CO_2-evoked activity of RIG, RIA, and AIY. Furthermore, we found that AIB does not show CO_2-evoked activity in animals raised at ambient or high CO_2 (Figure S3D), suggesting that the phenotypes of the AIB- AIZ- animals are attributable to AIZ. However, we cannot exclude the possibility that AIB contributes indirectly to CO_2 response in combination with AIZ. Together with our behavioral data showing that silencing AIZ enhances both CO_2 attraction and repulsion (Figures 2F, 3E), these results demonstrate that AIZ regulates behavioral sensitivity to CO_2 regardless of valence. Thus, distinct interneurons regulate valence and sensitivity.

A combinatorial code of neuropeptides regulates valence and sensitivity

The rapid shift in CO_2 response valence that occurs following a change in environmental CO_2 levels is consistent with a mechanism of valence encoding that involves neuromodulation rather than synaptic rewiring [49–51]. To gain insight into the neuromodulators that regulate CO_2 response valence, we examined the CO_2-evoked behaviors of animals lacking individual neuropeptides that were previously shown to be enriched in BAG [20]. We first examined the CO_2 response of animals raised at ambient CO_2 and found that animals lacking the FMRFamide-like neuropeptide FLP-27 showed reduced avoidance, while animals lacking the neuropeptide-like protein NLP-1 showed enhanced avoidance (Figure S4A–B). We then examined the CO_2 response of animals raised at high CO_2 and found that animals lacking FLP-27 showed reduced attraction, while animals lacking FLP-16 showed enhanced attraction (Figure S4C–D). These data suggest that FLP-16 reduces CO_2 attraction, NLP-1 reduces CO_2 repulsion, and FLP-27 enhances CO_2 response regardless of valence. Thus, different neuropeptides play distinct roles in regulating CO_2 response valence and sensitivity. Our results raise the intriguing possibility that BAG secretes different combinations of neuropeptides in animals raised at ambient vs. high CO_2 to generate experience-appropriate responses to CO_2. Activity-dependent regulation of neuropeptide expression has been demonstrated in BAG, where *flp-19* expression is greatly reduced in the absence of the CO_2-sensing pathway [52]. However, these neuropeptides may also act in other neurons to regulate the CO_2 circuit. Alternatively, modulation of the CO_2 circuit could be achieved through changes in receptor expression in the postsynaptic AIY, RIA and RIG interneurons, or modulatory input from other neurons.

A novel mechanism of valence encoding

We have examined the neural basis of CO_2 response and found that both CO_2 attraction and repulsion are mediated by a single microcircuit consisting of the BAG sensory neurons and four postsynaptic interneuron pairs: AIY, AIZ, RIA, and RIG (Figure 4E). CO_2 avoidance results from activation of RIA and RIG, and inhibition of AIY. CO_2 attraction results from activation of AIY, inhibition of RIA, and silencing of RIG. The valence associated with activation of each interneuron does not change as a result of experience: activation of AIY is always correlated with CO_2 attraction, and activation of RIA and RIG is always correlated with CO_2 avoidance. However, our data demonstrate that CO_2 response is determined by the combined activity states of AIY, RIA and RIG, and not solely by the interneuron(s) whose activation is correlated with its valence. The fourth interneuron pair, AIZ, regulates sensitivity regardless of valence. Furthermore, a combinatorial code of neuropeptides acts on the CO_2 circuit to regulate valence and sensitivity. Thus, the specific behavioral response to CO_2 is determined by the coordinated activity of four interneuron types, two of which are capable of showing both CO_2-evoked excitation and CO_2-evoked inhibition.

CO_2-evoked behaviors are also subject to modulation in other organisms. For example, CO_2 avoidance by the fruit fly *Drosophila melanogaster* and CO_2 attraction by the mosquito *Aedes aegypti* are reduced in the presence of food odorants through direct inhibition of CO2-detecting sensory neurons [53, 54]. CO_2 avoidance in *D. melanogaster* can also be attenuated by food odors through a mechanism in which the pathway mediating the response to food odors and the pathway mediating CO_2 response converge in the mushroom body [55,

56]. In addition, CO_2 is aversive to walking flies but attractive to flying flies, and different sets of chemoreceptors are required in the two conditions [57]. Thus, CO_2 response can be modulated by a number of different mechanisms across phyla.

In both invertebrates and vertebrates, a common mechanism for determining chemosensory valence involves two separate pathways, one that promotes attraction and one that promotes repulsion. Valence is then determined by which of these opposing pathways is activated [3, 58]. Here, we describe a novel mechanism of valence determination that instead involves a single pathway of interneurons. The CO_2-evoked activity of these interneurons is subject to extreme experience-dependent modulation based on the animal's recent exposure to CO_2, allowing them to contribute to both attractive and aversive responses to CO_2 (Figure 4E). Thus, the functional connectivity of sensory neuron to interneuron synapses rapidly changes to reflect the current ethological state of the animal. Valence-encoding interneurons have been identified in mammals [3, 59], but whether their activity is modulated to drive changes in innate valence has not yet been investigated. Our finding that *C. elegans* can generate opposite behavioral responses to the same chemosensory input as a result of experience-dependent modulation of sensory neuron to interneuron synapses raises the possibility that similar mechanisms operate in mammals to mediate rapid changes in innate valence.

STAR Methods

CONTACT FOR REAGENT AND RESOURCE SHARING

Further information and requests for strains and reagents should be directed to and will be fulfilled by the Lead Contact, Dr. Elissa Hallem (ehallem@ucla.edu).

EXPERIMENTAL MODEL AND SUBJECT DETAILS

The free-living nematode *Caenorhabditis elegans* was used as the experimental model for this study. *C. elegans* has two sexes, hermaphrodites and males. Our experiments were carried out with hermaphrodites; males were used only for crosses. Unless otherwise noted, all experiments were done using *C. elegans* young adults. Strains were maintained at room temperature (RT, ~22°C) and ambient CO_2 (0.038% CO_2) on Nematode Growth Media (NGM) plates containing a thin lawn of *Escherichia coli* OP50 bacteria, according to standard methods [60]. Strains raised at high CO_2 were placed in a Tritech Research DigiTherm® CO_2 heating/cooling incubator, at 22°C and 2.5% CO_2, for one generation and subsequently tested. Strains transferred from ambient CO_2 to high CO_2CO_2 were maintained at RT and ambient CO_2, and transferred to the CO_2 incubator (22°C; 2.5% CO_2) for the indicated amount of time. Strains transferred from high CO_2 to ambient CO_2 were maintained at RT and ambient CO_2, raised in the CO_2 incubator (22°C; 2.5% CO_2) for one generation, and subsequently transferred to RT and ambient CO_2 for the indicated amount of time. All transgenic strains were made by microinjection of plasmid DNA into N2 hermaphrodites. See Key Resources Table for details.

EAH202 was obtained from Y. Iino (University of Tokyo, Tokyo, Japan) and then given an EAH strain number for identification purposes. EAH284 was generated by microinjecting the following plasmids, obtained from D. Colón-Ramos: DACR335 *ttx-3::casp-3(p17)* and

DACR336 *ttx- 3::casp-3(p12)*. EAH314 was derived from VM4770 [42] by outcrossing to N2 for 3 generations. The following strains were used to confirm results with independent transgenes: TV2217, EAH319, EAH267, and EAH346. TV2217 was obtained from D. Colón-Ramos [61]. The AIY ablation phenotype was confirmed using strain OH8, which contains a *ttx-3* mutation. EAH319 was generated by microinjecting the following plasmids, obtained from D. Colón-Ramos: DACR77 *glr-3::casp-3(p17)* and DACR76 *glr-3::casp-3(p12)*. The following GFP reporter strains were used to confirm cell ablations: OH99, EAH242, EAH269, IK716. EAH242 and EAH269 were generated using pCZGY#1534, obtained from Y. Jin [62]. The following strains were used to confirm results with independent deletion alleles: FX04829, RB2275, RB1902, FX04612, RB1340. The following strains were tested to rule out the possibility that the phenotypes observed with VC2012 were due to a deletion in *Y17G7B.22* rather than *flp-27:* VC2180 and VC2063. The AIB AIZ-silenced strain IV316 was obtained from S. Chalasani [63]. Calcium imaging of AIY and AIZ was performed using strains IK1405 and IK686, respectively, which were obtained from I. Mori [64, 65]. Calcium imaging of RIA was performed using strain AX2361, which was obtained from M. de Bono [48]. Calcium imaging of AIB was performed using EAH259, which was obtained from T. Hirotsu [66].

METHOD DETAILS

CO_2 chemotaxis assays—Chemotaxis assays were performed as previously described (Figure S1A) [12]. Young adult animals were washed off plates using M9 buffer [60] and collected into a 65-mm Syracuse watch glass. Animals were washed 3x with M9 buffer and transferred to a 1-cm × 1-cm square of Whatman paper. Animals were then transferred from the filter paper to the center of a 100-mm NGM or chemotaxis plate [67]. The actual potential crawling distance of the animals is the diameter of the inside base of the plate, which measures 84.4 mm. A CO_2 gradient was generated by delivering gas stimuli to the plate through holes in the plate lids as previously described [12]. Unless otherwise indicated, a 21% O_2, balance N2 air control was delivered through one hole, and a certified mixture containing a designated CO_2 concentration with 21% O_2 and the balance N2 (Airgas) was delivered through the other hole. Gases were pumped through ¼-inch flexible PVC tubing using a syringe pump (PHD 2000, Harvard Apparatus) at a rate of 2 mL/min. The duration of the assay was 20 min. The number of animals in a 20-mm diameter circle centered under each gas inlet was counted and used to determine the chemotaxis index (CI), according to the formula:

$$CI = \frac{\#\,of\ animals\ at\ CO_2 - \#\,of\ animals\ at\ air\ control}{\#\,of\ animals\ at\ CO_2 + air\ control}$$

To control for directional bias due to subtle room vibrations, two identical assays were always performed simultaneously with the CO_2 gradient in opposite directions. Assays were discarded if the difference in the CI for the two plates was >0.9 or if fewer than 7 worms moved into the scoring regions on either plate. Transgenic strains expressing the histamine-gated chloride channel HisCl1 were incubated on NGM plates containing 10 mM histamine but not *E. coli* OP50 [45] for 20 min prior to the chemotaxis assay.

For assays where animals were raised at ambient CO_2 and transferred to high (2.5%) CO_2, the extent to which the animals had switched valence to attraction was calculated for each trial by comparing the CI for the current trial to the mean CIs for animals of the same genotype cultivated at either ambient or high CO_2 according to the following formula:

$$\%\ change\ in\ valence\ = \frac{CI\ for\ current\ trial\ -\ mean\ CI\ for\ ambient\ CO_2\ trials}{mean\ CI\ for\ high\ CO_2\ trials\ -\ mean\ CI\ for\ ambient\ CO_2\ trials} \times 100$$

For assays where the animals were raised at high CO_2 and transferred to ambient CO_2, the extent to which the animals had switched valence to avoidance was calculated for each trial by comparing the CI for the current trial to the mean CIs for animals of the same genotype cultivated at either ambient or high CO_2 according to the following formula:

$$\%\ change\ in\ valence\ = \frac{mean\ CI\ for\ ambient\ CO_2\ trials\ -\ CI\ for\ current\ trial}{mean\ CI\ for\ high\ CO_2\ trials\ -\ mean\ CI\ for\ ambient\ CO_2\ trials} \times 100$$

Values below 0 were counted as 0. Values greater than 100 were counted as 100.

Calcium imaging—Imaging was performed as previously described [12] using the genetically encoded calcium indicators yellow cameleon YC2.12 and YC3.60 [68]. Young adults were immobilized onto a cover glass containing a 2% agarose pad made with 10 mM HEPES using Butler Schein Animal Health Surgi-lock 2-octyl cyanoacrylate instant tissue adhesive. A custom-made gas delivery chamber was secured over the cover glass. Gases were delivered at a rate of 0.7–0.8 L/min. During the assay, 20 s of 21% O_2 was followed by a 20-s pulse of 15% CO_2, followed by 20 s of 21% O_2. Imaging was performed on a Zeiss AxioObserver A1 inverted microscope using a 40X EC Plan-NEOFLUAR lens, a Hamamatsu C9100 EM-CCD camera, and AxioVision software. The EM gain was set at 30. The emission image was passed through a DV2 beam splitter (Photometrics) as previously described [12]. Image analysis was performed using Zeiss AxioVision Software and Microsoft Excel.

For each recording, the mean pixel value of a background region of interest was subtracted from the mean pixel value of a region of interest containing the neuron soma (RIG, AIZ, AIB) or neuron process (AIY, RIA). When imaging from AIY, we focused on the synapse-rich segment of the process designated zone 2 [69]. When imaging from RIA, we focused primarily on the “loop” segment of the RIA process, and occasionally on nrV, the ventral segment of the process in the nerve ring [70]. Fluorescence values were normalized to the average values obtained 10 s prior to CO_2 delivery. The YFP/CFP ratio was calculated as previously described [20]. Images were baseline-corrected using a linear baseline correction. Traces with unstable baselines prior to the onset of the CO_2 pulse were discarded. To establish appropriate criteria for including traces as either depolarizations or hyperpolarizations, we recorded control traces for each genotype using a 21% O_2, balance N2 air control pulse. We then calculated the standard deviation of the set containing the maximum value of each control trace (max set), and the standard deviation of the set containing the minimum value of each control trace (min set). Traces recorded with a CO_2

pulse where the maximum value exceeded 3 standard deviations from the mean of the air control (max set) were designated depolarizations; traces recorded with a CO_2 pulse where the minimum value exceeded 3 standard deviations from the mean of the air control (min set) were designated hyperpolarizations. For cases where we observed CO_2-evoked depolarizations or hyperpolarizations, traces where the maximum or minimum value, respectively, was within 3 standard deviations of the mean of the max or min set for the air control were discarded.

For imaging animals raised at high CO_2, animals were incubated at 2.5% CO_2 for one generation. Prior to imaging, cameleon-expressing animals were placed on individual plates so they could subsequently be removed from the incubator one at a time to minimize time at ambient CO_2. Immediately prior to recording, individual animals were removed from the incubator and then prepared for imaging, spending approximately 5 min at ambient CO_2 before imaging. We note that for all imaging experiments, the CO_2 concentrations used for calcium imaging cannot be directly compared to the CO_2 concentrations used for behavioral assays due to differences in the setup for CO_2 delivery in the two cases.

Fluorescence microscopy—Images of gcy-9::GFP-expressing animals were acquired as previously described [12]. Animals were selected at the L4 stage using the co-injection marker *pax-2::GFP. pax-2* expression is visible in the vulva at the L4 stage [71]. Selection based on *pax-2* expression was used to limit bias and obtain a representative sample of *gcy-9* expression.

Molecular biology—To achieve BAG-specific expression of *pkc-1(gf)*, a 3-kb sequence upstream of the *flp-17* gene [31, 72] was PCR-amplified from genomic DNA using primers 5′-gcggccgcaaaattatctggattcaccaac-3′ and 5′-ggatccggaaaatatttccacacagaat-3′, and used to drive expression of *pkc-1(gf)* [44]. A plasmid containing the *pkc-1(gf)* sequence was obtained from C. Bargmann (Rockefeller University, NY). AIY-specific expression of *pkc-1(gf)* was achieved using a 4-kb region of the *ttx-3* gene [69, 73] that was PCR-amplified from genomic DNA using primers 5′-gcggccgcaagctttttgaaacgatctt-3′ and 5′-ggatccatttgacaccgaagacaatt-3′. RIG-specific expression of *pkc-1(gf)* was achieved using a 149-bp region of the *twk-3* promoter [74]. A plasmid containing the *twk-3* promoter sequence was obtained from L. Salkoff (Washington University, MO). RIA-specific expression of *pkc-1(gf)* was achieved using a 1.2-kb region of the *glr-3* gene [70] that was PCR-amplified from genomic DNA using primers 5′-gcatgcatcactgagccagagatgag-3′ and 5′-ggatccatgttaatagcaaatattgaagattc-3′. To generate a BAG-specific rescue of *eat-4*, we obtained a plasmid from I. Mori (Nagoya University, Japan) containing *eat-4* cDNA. *eat-4* cDNA was PCR-amplified from the plasmid using the following primers 5′-gctagccatgtcgtcatggaacgag-3′ and 5′-ggtaccagatggcgatctgatgacag-3′. Using our previously generated *flp-17::pkc- 1(gf)::SL2::GFP* plasmid, we replaced the *pkc-1(gf)* sequence with the *eat-4* cDNA sequence and injected the resulting *flp-17::eat-4::SL2::GFP* plasmid into the MT6308 *eat-4(ky5)* strain, at 50 ng/**μ**L. Behavioral results were confirmed with two independently derived rescue lines.

Interneuron ablation strains were generated using the two-component reconstituted caspase system previously described [75]. For genetic ablation of AIY, the following plasmids were

obtained from D. Colón-Ramos (Yale University): DACR335 *ttx-3::casp-3(p17)* and DACR336 *ttx- 3::casp-3(p12)* [69, 73]. For genetic ablation of RIB, cell-specific expression was achieved using the *cex-1* promoter [69]. A 1 -kb sequence upstream of *cex-1* was PCR-amplified from genomic DNA using primers 5 ′-gtcgacttttaaatggaaagtaaaacga-3 ′ and 5 ′-ggatccttctgaaagtataagatttgactga-3 ′. The *cex-1* sequence, along with DACR335 and DACR336, were used to generate *cex-1::casp- 3(p17)* and *cex-1::casp-3(p12)*. For genetic ablation of RIG, cell-specific expression was achieved using the same 149-bp promoter region of *twk-3* used to generate *RIG::pkc-1(gf)* (described above). The *twk-3* sequence, along with DACR335 and DACR336, were used to make *twk- 3::casp-3(p17)* and *twk-3::casp-3(p12)*. For genetic ablation of RIA, cell-specific expression was achieved using the promoter region of the *glr-3* gene [70]. The following plasmids were obtained from D. Colón-Ramos (Yale University): DACR77 *glr-3::casp-3(p17)* and DACR76 *glr-3::casp-3(p12)*. Plasmids were injected at 50 ng/**μ**L (AIY), 15 ng/**μ**L (RIB), 35 ng/**μ**L (RIG) or 35 ng/**μ**L (RIA), along with the coinjection marker *myo-2::dsRed* (10 ng/**μ**L), using standard microinjection techniques. Stable transgenic lines expressing *myo-2::dsRed* were crossed to the following GFP reporter strains to confirm loss of the respective interneurons: OH99 (AIY), EAH243 (RIB), EAH269 (RIG), and IK716 (RIA).

QUANTIFICATION AND STATISTICAL ANALYSIS

Statistical analysis was performed using GraphPad Prism 6 using standard significance tests. Significance values were calculated relative to the N2 control, unless otherwise indicated. All statistical details for each experiment can be found in the figure legends. The D'Agostino-Pearson omnibus normality test was used to determine whether values came from a Gaussian distribution; if data were not normally distributed, non-parametric tests were used.

Supplementary Material

Refer to Web version on PubMed Central for supplementary material.

Acknowledgments

We thank C. Bargmann (Rockefeller University, NY), M. de Bono (Cambridge, UK), Y. Iino (University of Tokyo, Japan), S. Chalasani (UCSD, CA), D. Biron (University of Chicago, IL), A. Maricq (University of Utah, UT), D. Colón-Ramos (Yale University, CT), I. Mori (Nagoya University, Japan), Y. Jin (UCSD, CA), L. Salkoff (Washington University, MO), S. Mitani (TWMU, Japan), T. Hirotsu (Kyushu University, Japan), and the *Caenorhabditis* Genetics Center for *C. elegans* strains and plasmids. We also thank J. Peña for assisting with molecular biology; and A. Bryant, S. Rengarajan, K. Yankura, and M. Frye for insightful comments on the manuscript. This work was supported by an NSF Graduate Research Fellowship (DGE-1144087) and an NIH Ruth L. Kirschstein National Research Service Award (GM007185) to M.L.G.; an NSF Graduate Research Fellowship (DGE-0707424) and a Eugene V. Cota-Robles Fellowship to M.A.C.; and an NSF Division of Integrative Organismal Systems grant (IOS-1456064), a McKnight Scholar Award, and an HHMI Faculty Scholar Award to E.A.H.

References

1. Mennella JA, Pepino MY, and Reed DR (2005). Genetic and environmental determinants of bitter perception and sweet preferences. Pediatrics 115, e216–e222. [PubMed: 15687429]

2. O'Doherty J, Rolls ET, Francis S, Bowtell R, McGlone F, Kobal G, Renner B, and Ahne G (2000). Sensory-specific satiety-related olfactory activation of the human orbitofrontal cortex. Neuroreport 11, 893–897. [PubMed: 10757540]
3. Li Q, and Liberles SD Aversion and attraction through olfaction. Curr Biol 25, R120–129. [PubMed: 25649823]
4. Lee J, Dillman AR, and Hallem EA (2016). Temperature-dependent changes in the host-seeking behaviors of parasitic nematodes. BMC Biol 14, 36. [PubMed: 27154502]
5. Kimata T, Sasakura H, Ohnishi N, Nishio N, and Mori I (2012). Thermotaxis of *C. elegans* as a model for temperature perception, neural information processing and neural plasticity. Worm 1, 31–41. [PubMed: 24058821]
6. Mengoni SL, Lorenzo-Figueiras AN, and Minoli SA (2017). Experience-dependent modulation of the attraction to faeces in the kissing bug *Triatoma infestans*. J Insect Physiol 98, 23–28. [PubMed: 27840288]
7. Chao MY, Komatsu H, Fukuto HS, Dionne HM, and Hart AC (2004). Feeding status and serotonin rapidly and reversibly modulate a *Caenorhabditis elegans* chemosensory circuit. Proc Natl Acad Sci USA 101, 15512–15517. [PubMed: 15492222]
8. Sengupta P (2013). The belly rules the nose: feeding state-dependent modulation of peripheral chemosensory responses. Curr Opin Neurobiol 23, 68–75. [PubMed: 22939570]
9. Sakai N, Iwata R, Yokoi S, Butcher RA, Clardy J, Tomioka M, and Iino Y (2013). A sexually conditioned switch of chemosensory behavior in *C. elegans*. PLoS ONE 8, e68676. [PubMed: 23861933]
10. Scott K (2011). Out of thin air: sensory detection of oxygen and carbon dioxide. Neuron 69, 194–202. [PubMed: 21262460]
11. Ma DK, and Ringstad N (2012). The neurobiology of sensing respiratory gases for the control of animal behavior. Front Biol (Beijing) 7, 246–253. [PubMed: 22876258]
12. Carrillo MA, Guillermin ML, Rengarajan S, Okubo R, and Hallem EA (2013). O_2-sensing neurons control CO_2 response in *C. elegans*. J Neurosci 33, 9675–9683. [PubMed: 23739964]
13. Brandt JP, and Ringstad N (2015). Toll-like receptor signaling promotes development and function of sensory neurons required for a *C. elegans* pathogen-avoidance behavior. Curr Biol 25, 2228–2237. [PubMed: 26279230]
14. Burg SP, and Burg EA (1965). Gas exchange in fruits. Physiol Plant 18, 870–884.
15. Hallem EA, and Sternberg PW (2008). Acute carbon dioxide avoidance in *Caenorhabditis elegans*. Proc Natl Acad Sci uSa 105, 8038–8043. [PubMed: 18524955]
16. Bretscher AJ, Busch KE, and de Bono M (2008). A carbon dioxide avoidance behavior is integrated with responses to ambient oxygen and food in *Caenorhabditis elegans*. Proc Natl Acad Sci USA 105, 8044–8049. [PubMed: 18524954]
17. Hedgecock EM, and Russell RL (1975). Normal and mutant thermotaxis in the nematode *Caenorhabditis elegans*. Proc Natl Acad Sci USA 72, 4061–4065. [PubMed: 1060088]
18. Kunitomo H, Sato H, Iwata R, Satoh Y, Ohno H, Yamada K, and Iino Y (2013). Concentration memory-dependent synaptic plasticity of a taste circuit regulates salt concentration chemotaxis in *Caenorhabditis elegans*. Nat Commun 4, 2210. [PubMed: 23887678]
19. Sharabi K, Hurwitz A, Simon AJ, Beitel GJ, Morimoto RI, Rechavi G, Sznajder JI, and Gruenbaum Y (2009). Elevated CO_2 levels affect development, motility, and fertility and extend life span in *Caenorhabditis elegans*. Proc Natl Acad Sci USA 106, 40244029. [PubMed: 19237558]
20. Hallem EA, Spencer WC, McWhirter RD, Zeller G, Henz SR, Ratsch G, Miller DM, Horvitz HR, Sternberg PW, and Ringstad N (2011). Receptor-type guanylate cyclase is required for carbon dioxide sensation by *Caenorhabditis elegans*. Proc Natl Acad Sci USA 108, 254–259. [PubMed: 21173231]
21. Sieburth D, Madison JM, and Kaplan JM (2007). PKC-1 regulates secretion of neuropeptides. Nat Neurosci 10, 49–57. [PubMed: 17128266]
22. Sieburth D, Ch'ng Q, Dybbs M, Tavazoie M, Kennedy S, Wang D, Dupuy D, Rual JF, Hill DE, Vidal M, et al. (2005). Systematic analysis of genes required for synapse structure and function. Nature 436, 510–517. [PubMed: 16049479]

23. Brandt JP, Aziz-Zaman S, Juozaityte V, Martinez-Velazquez LA, Petersen JG, Pocock R, and Ringstad N (2012). A single gene target of an ETS-family transcription factor determines neuronal CO2-chemosensitivity. PLoS ONE 7, e34014. [PubMed: 22479504]
24. Smith ES, Martinez-Velazquez L, and Ringstad N (2013). A chemoreceptor that detects molecular carbon dioxide. J Biol Chem 288, 37071–37081. [PubMed: 24240097]
25. Guillermin ML, Castelletto ML, and Hallem EA (2011). Differentiation of carbon dioxide-sensing neurons in *Caenorhabditis elegans* requires the ETS-5 transcription factor. Genetics 189, 1327–1339. [PubMed: 21954162]
26. Dalton P (2000). Psychophysical and behavioral characteristics of olfactory adaptation. Chem Senses 25, 487–492. [PubMed: 10944515]
27. Sachse S, Rueckert E, Keller A, Okada R, Tanaka NK, Ito K, and Vosshall LB (2007). Activity-dependent plasticity in an olfactory circuit. Neuron 56, 838–850. [PubMed: 18054860]
28. Dennis CE, Adhikari S, Wright AW, and Suski CD (2016). Molecular, behavioral, and performance responses of juvenile largemouth bass acclimated to an elevated carbon dioxide environment. J Comp Physiol B 186, 297–311. [PubMed: 26758610]
29. Bargmann CI (2006). Chemosensation in C. elegans. In WormBook, www.WormBook.org.
30. Zimmer M, Gray JM, Pokala N, Chang AJ, Karow DS, Marletta MA, Hudson ML, Morton DB, Chronis N, and Bargmann CI (2009). Neurons detect increases and decreases in oxygen levels using distinct guanylate cyclases. Neuron 61, 865–879. [PubMed: 19323996]
31. Ringstad N, and Horvitz HR (2008). FMRFamide neuropeptides and acetylcholine synergistically inhibit egg-laying by *C. elegans*. Nat Neurosci 11, 1168–1176. [PubMed: 18806786]
32. Peymen K, Watteyne J, Frooninckx L, Schoofs L, and Beets I (2014). The FMRFamide-like peptide family in nematodes. Front Endocrinol (Lausanne) 5, 90. [PubMed: 24982652]
33. Serrano-Saiz E, Poole RJ, Felton T, Zhang F, De La Cruz ED, and Hobert O (2013). Modular control of glutamatergic neuronal identity in *C. elegans* by distinct homeodomain proteins. Cell 155, 659–673. [PubMed: 24243022]
34. White JG, Southgate E, Thomson JN, and Brenner S (1986). The structure of the nervous system of the nematode *Caenorhabditis elegans*. Philos Trans R Soc Lond B Biol Sci 314, 1–340. [PubMed: 22462104]
35. Xu M, Jarrell TA, Wang Y, Cook SJ, Hall DH, and Emmons SW (2013). Computer assisted assembly of connectomes from electron micrographs: application to *Caenorhabditis elegans*. PLoS ONE 8, e54050. [PubMed: 23342070]
36. Chalasani SH, Chronis N, Tsunozaki M, Gray JM, Ramot D, Goodman MB, and Bargmann CI (2007). Dissecting a circuit for olfactory behaviour in *Caenorhabditis elegans*. Nature 450, 63–70. [PubMed: 17972877]
37. Chronis N, Zimmer M, and Bargmann CI (2007). Microfluidics for in vivo imaging of neuronal and behavioral activity in *Caenorhabditis elegans*. Nat Methods 4, 727–731. [PubMed: 17704783]
38. Yu S, Avery L, Baude E, and Garbers DL (1997). Guanylyl cyclase expression inspecific sensory neurons: a new family of chemosensory receptors. Proc Natl Acad USA 94, 3384–3387.
39. Ha HI, Hendricks M, Shen Y, Gabel CV, Fang-Yen C, Qin Y, Colon-Ramos D, Shen K, Samuel AD, and Zhang Y (2010). Functional organization of a neural network for aversive olfactory learning in *Caenorhabditis elegans*. Neuron 68, 1173–1186. [PubMed: 21172617]
40. Singh K, Chao MY, Somers GA, Komatsu H, Corkins ME, Larkins-Ford J, Tucey T, Dionne HM, Walsh MB, Beaumont EK, et al. (2011). *C. elegans* Notch signaling regulates adult chemosensory response and larval molting quiescence. Curr Biol 21, 825834. [PubMed: 21549604]
41. Tsalik EL, and Hobert O (2003). Functional mapping of neurons that control locomotory behavior in *Caenorhabditis elegans*. J Neurobiol 56, 178–197. [PubMed: 12838583]
42. Zheng Y, Brockie PJ, Mellem JE, Madsen DM, and Maricq AV (1999). Neuronal control of locomotion in *C. elegans* is modified by a dominant mutation in the GLR-1 ionotropic glutamate receptor. Neuron 24, 347–361. [PubMed: 10571229]
43. Schiavo G, Benfenati F, Poulain B, Rossetto O, Polverino de Laureto P, DasGupta BR, and Montecucco C (1992). Tetanus and botulinum-B neurotoxins block neurotransmitter release by proteolytic cleavage of synaptobrevin. Nature 359, 832–835. [PubMed: 1331807]

44. Macosko EZ, Pokala N, Feinberg EH, Chalasani SH, Butcher RA, Clardy J, and Bargmann CI (2009). A hub-and-spoke circuit drives pheromone attraction and social behaviour in *C. elegans*. Nature 458, 1171–1175. [PubMed: 19349961]
45. Pokala N, Liu Q, Gordus A, and Bargmann CI (2014). Inducible and titratable silencing of *Caenorhabditis elegans* neurons *in vivo* with histamine-gated chloride channels. Proc Natl Acad Sci USA 111, 2770–2775. [PubMed: 24550306]
46. Jin X, Pokala N, and Bargmann CI (2016). Distinct circuits for the formation and retrieval of an imprinted olfactory memory. Cell 164, 632–643. [PubMed: 26871629]
47. Ohnishi N, Kuhara A, Nakamura F, Okochi Y, and Mori I (2011). Bidirectional regulation of thermotaxis by glutamate transmissions in *Caenorhabditis elegans*. Embo J 30, 1376–1388. [PubMed: 21304490]
48. Kodama-Namba E, Fenk LA, Bretscher AJ, Gross E, Busch KE, and de Bono M (2013). Cross-modulation of homeostatic responses to temperature, oxygen and carbon dioxide in *C. elegans*. PLoS Genet 9, e1004011. [PubMed: 24385919]
49. Dickinson PS (2006). Neuromodulation of central pattern generators in invertebrates and vertebrates. Curr Opin Neurobiol 16, 604–614. [PubMed: 17085040]
50. Lee SH, and Dan Y (2012). Neuromodulation of brain states. Neuron 76, 209–222. [PubMed: 23040816]
51. Bargmann CI (2012). Beyond the connectome: how neuromodulators shape neural circuits. Bioessays 34, 458–465. [PubMed: 22396302]
52. Rojo Romanos T, Petersen JG, and Pocock R (2017). Control of neuropeptide expression by parallel activity-dependent pathways in *Caenorhabditis elegans*. Sci Rep 7, 38734. [PubMed: 28139692]
53. Turner SL, and Ray A (2009). Modification of CO_2 avoidance behaviour in *Drosophila* by inhibitory odorants. Nature 461, 277–281. [PubMed: 19710651]
54. Turner SL, Li N, Guda T, Githure J, Carde RT, and Ray A (2011). Ultra-prolonged activation of CO_2-sensing neurons disorients mosquitoes. Nature 474, 87–91. [PubMed: 21637258]
55. Bracker LB, Siju KP, Varela N, Aso Y, Zhang M, Hein I, Vasconcelos ML, and Grunwald Kadow IC (2013). Essential role of the mushroom body in context-dependent CO_2 avoidance in Drosophila. Curr Biol 23, 1228–1234. [PubMed: 23770186]
56. Lewis LP, Siju KP, Aso Y, Friedrich AB, Bulteel AJ, Rubin GM, and Grunwald Kadow IC (2015). A higher brain circuit for immediate integration of conflicting sensory information in *Drosophila*. Curr Biol 25, 2203–2214. [PubMed: 26299514]
57. Wasserman S, Salomon A, and Frye MA (2013). *Drosophila* tracks carbon dioxide in flight. Curr Biol 23, 301–306. [PubMed: 23352695]
58. Knaden M, and Hansson BS (2014). Mapping odor valence in the brain of flies and mice. Curr Opin Neurobiol 24, 34–38. [PubMed: 24492076]
59. Root CM, Denny CA, Hen R, and Axel R (2014). The participation of cortical amygdala in innate, odour-driven behaviour. Nature 515, 269–273. [PubMed: 25383519]
60. Stiernagle T (2006). Maintenance of *C. elegans*. In WormBook, www.WormBook.org.
61. Luo L, Cook N, Venkatachalam V, Martinez-Velazquez LA, Zhang X, Calvo AC, Hawk J, MacInnis BL, Frank M, Ng JH, et al. (2014). Bidirectional thermotaxis in *Caenorhabditis elegans* is mediated by distinct sensorimotor strategies driven by the AFD thermosensory neurons. Proc Natl Acad Sci USA 111, 2776–2781. [PubMed: 24550307]
62. Qi YB, Garren EJ, Shu X, Tsien RY, and Jin Y (2012). Photo-inducible cell ablation in *Caenorhabditis elegans* using the genetically encoded singlet oxygen generating protein miniSOG. Proc Natl Acad Sci USA 109, 7499–7504. [PubMed: 22532663]
63. Calhoun AJ, Tong A, Pokala N, Fitzpatrick JA, Sharpee TO, and Chalasani SH (2015). Neural mechanisms for evaluating environmental variability in *Caenorhabditis elegans*. Neuron 86, 428–441. [PubMed: 25864633]
64. Kuhara A, and Mori I (2006). Molecular physiology of the neural circuit for calcineurin-dependent associative learning in *Caenorhabditis elegans*. J Neurosci 26, 9355–9364. [PubMed: 16971519]

65. Kuhara A, Ohnishi N, Shimowada T, and Mori I (2011). Neural coding in a single sensory neuron controlling opposite seeking behaviours in *Caenorhabditis elegans*. Nat Commun 2, 355. [PubMed: 21673676]

66. Uozumi T, Hirotsu T, Yoshida K, Yamada R, Suzuki A, Taniguchi G, Iino Y, and Ishihara T (2012). Temporally-regulated quick activation and inactivation of Ras is important for olfactory behaviour. Sci Rep 2, 500. [PubMed: 22787558]

67. Bargmann CI, Hartwieg E, and Horvitz HR (1993). Odorant-selective genes and neurons mediate olfaction in *C. elegans*. Cell 74, 515–527. [PubMed: 8348618]

68. Nagai T, Yamada S, Tominaga T, Ichikawa M, and Miyawaki A (2004). Expanded dynamic range of fluorescent indicators for Ca2+ by circularly permuted yellow fluorescent proteins. Proc Natl Acad Sci USA 101, 10554–10559. [PubMed: 15247428]

69. Colon-Ramos DA, Margeta MA, and Shen K (2007). Glia promote local synaptogenesis through UNC-6 (netrin) signaling in C. elegans. Science 318, 103–106. [PubMed: 17916735]

70. Hendricks M, Ha H, Maffey N, and Zhang Y (2012). Compartmentalized calcium dynamics in a *C. elegans* interneuron encode head movement. Nature 487, 99–103. [PubMed: 22722842]

71. Fernandes JS, and Sternberg PW (2007). The tailless ortholog *nhr-67* regulates patterning of gene expression and morphogenesis in the *C. elegans* vulva. PLoS Genet 3, e69. [PubMed: 17465684]

72. Li C, and Kim K (2008). Neuropeptides. In WormBook, www.WormBook.org.

73. Clark DA, Biron D, Sengupta P, and Samuel AD (2006). The AFD sensory neurons encode multiple functions underlying thermotactic behavior in *Caenorhabditis elegans*. J Neurosci 26, 7444–7451. [PubMed: 16837592]

74. Salkoff L, Butler A, Fawcett G, Kunkel M, McArdle C, Paz-y-Mino G, Nonet M, Walton N, Wang ZW, Yuan A, et al. (2001). Evolution tunes the excitability of individual neurons. Neuroscience 103, 853–859. [PubMed: 11301195]

75. Chelur DS, and Chalfie M (2007). Targeted cell killing by reconstituted caspases. Proc Natl Acad Sci USA 104, 2283–2288. [PubMed: 17283333]

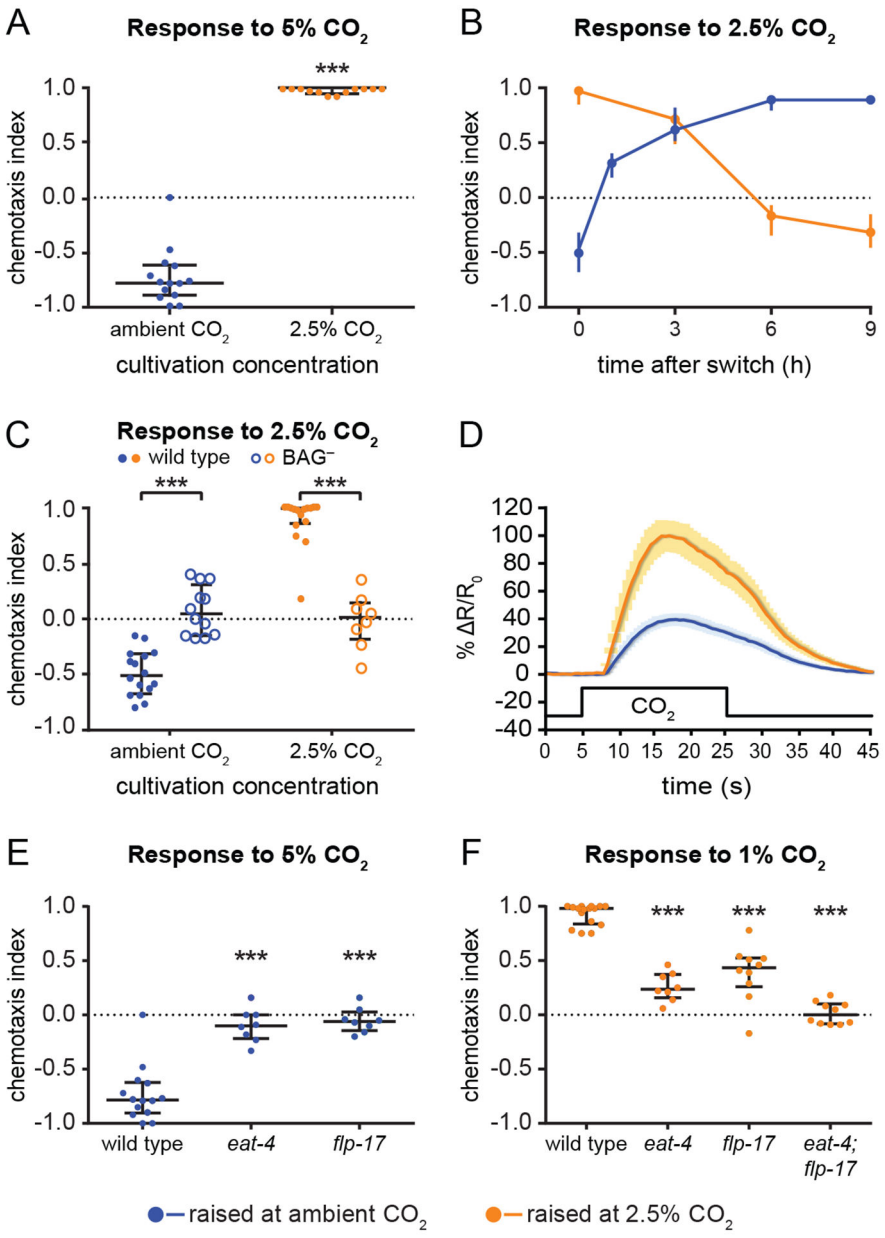

Figure 1. *C. elegans* shows both attractive and aversive responses to CO_2.

(A) Animals raised at ambient CO_2 (0.038%) avoid 5% CO_2, while animals raised at high (2.5%) CO_2 are attracted to 5% CO_2. ***p<0.001, Mann-Whitney test. n=12–14 trials per condition.

(B) Adults raised at ambient CO_2 were incubated at high (2.5%) CO_2 for 1, 3, 6, or 9 h and then assayed for their response to 2.5% CO_2 (blue), while adults raised at high CO_2 were put at ambient CO_2 for 3, 6, or 9 h and then assayed for their response to 2.5% CO_2 (orange). A switch in CO_2 environment triggers a rapid change in CO_2 response valence. n=8–24 trials per condition.

(C) BAG sensory neurons are required for CO_2 avoidance and attraction. Wild-type animals raised at ambient CO_2 avoid 2.5% CO_2, while wild-type animals raised at high (2.5%) CO_2

are attracted to 2.5% CO_2. BAG-ablated animals (BAG-) do not respond to CO_2 under either condition. ***p<0.001, two-way ANOVA with Sidak's post-test. n=8–16 trials per condition.

(D) BAG neurons of animals raised at high (2.5%) CO_2 respond more robustly to CO_2 than BAG neurons of animals raised at ambient CO_2. Graph shows the calcium responses of BAG to 15%CO_2, for animals raised at ambient CO_2 (blue) or high CO_2 (orange), measured using the ratiometric calcium indicator yellow cameleon YC3.60. Solid lines indicate average calcium responses; shading represents SEM. Black line indicates the CO_2 pulse. Animals raised at high CO_2 show an increased BAG response relative to animals raised at ambient CO_2 (***p<0.001, unpaired t test). n=10–15 animals per condition.

(E-F) *eat-4* and *flp-17* are required for normal CO_2 response. (E) Mutation of *eat-4* or *flp-17* abolishes CO_2 avoidance in animals raised at ambient CO_2. Responses shown are to 5% CO_2. ***p<0.001, Kruskal-Wallis test with Dunn's post-test. n=8–14 trials per genotype and condition.

(F) Mutation of either *eat-4* or *flp-17* reduces CO_2 attraction, and mutation of both genes abolishes CO_2 attraction, in animals raised at high (2.5%) CO_2. Responses shown are to 1% CO_2. ***p<0.001, one-way ANOVA with Dunnett's post-test. n=8–16 trials per genotype and condition.

For A-C, E and F, graphs depict medians with interquartile ranges. See also Figures S1 and S2.

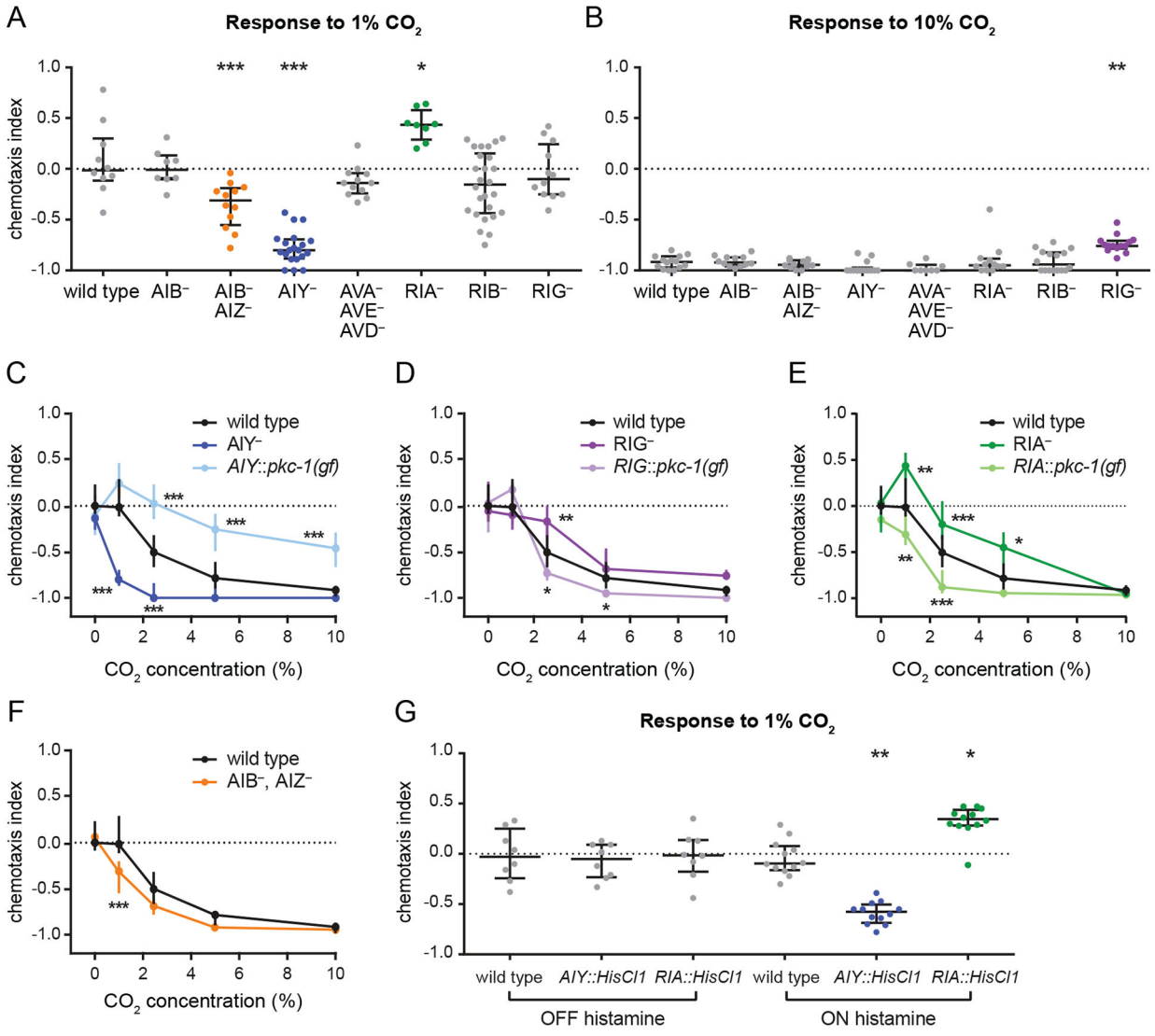

Figure 2. Distinct interneurons act in opposition to regulate CO_2 avoidance in animals raised at ambient CO_2.

(A-B) In animals raised at ambient CO_2, silencing of AIZ and ablation of AIY enhances CO_2 avoidance, ablation of RIG reduces CO_2 avoidance, and ablation of RIA results in CO_2 attraction. Animals were raised at ambient CO_2 and screened for responses to 1% CO_2 (A) and 10% CO_2

(B). Interneurons were either genetically ablated individually (AIB-, AIY-, RIA-, RIB-, and RIG-); genetically ablated simultaneously (AVA- AVE- AVD-); or silenced with tetanus toxin simultaneously (AIB- AIZ-). *p<0.05, **p<0.01, ***p<0.001, one-way ANOVA with Dunnett's posttest (A) or Kruskal-Wallis test with Dunn's post-test (B). n=8–26 trials per genotype and condition.

(C) Ablation of AIY enhances CO_2 avoidance. By contrast, animals with more active AIY neurons due to AIY-specific expression of *pkc-1(gf)* show reduced CO_2 avoidance. Animals were raised at ambient CO_2. ***p<0.001, two-way ANOVA with Dunnett's post-test. n=8–26 trials per genotype and condition.

(D) Ablation of RIG reduces CO_2 avoidance. By contrast, animals with more active RIG neurons due to RIG-specific expression of *pkc-1(gf)* show enhanced CO_2 avoidance. Animals were raised at ambient CO_2. *p<0.05, **p<0.01, two-way ANOVA with Dunnett's post-test. n=8–30 trials per genotype and condition.
(E) Ablation of RIA reduces CO_2 avoidance. By contrast, animals with more active RIA neurons due to RIA-specific expression of *pkc-1(gf)* show enhanced CO_2 avoidance. Animals were raised at ambient CO_2. *p<0.05, **p<0.01, ***p<0.001, two-way ANOVA with Dunnett's post-test. n=8–16 trials per genotype and condition.
(F) Silencing of AIZ enhances CO_2 avoidance. Animals were raised at ambient CO_2. ***p<0.001, two-way ANOVA with Sidak's post-test. n=8–16 trials per genotype and condition.
(G) Animals with AIY neurons transiently silenced by expression of the histamine-gated chloride channel HisCl1 in AIY show enhanced CO_2 avoidance. By contrast, animals with RIA neurons transiently silenced using the same approach show CO_2 attraction. Responses to 1% CO_2 were tested for wild-type animals and animals expressing HisCl1 in either AIY or RIA without histamine (negative control) and with histamine (neuronal silencing); changes in CO_2 response were observed only in the presence of histamine. Animals were raised at ambient CO_2. *p<0.05, ***p<0.001, Kruskal-Wallis test with Dunn's post-test. n=8–12 trials per genotype and condition.
For A-G, graphs show medians and interquartile ranges. See also Figure S3.

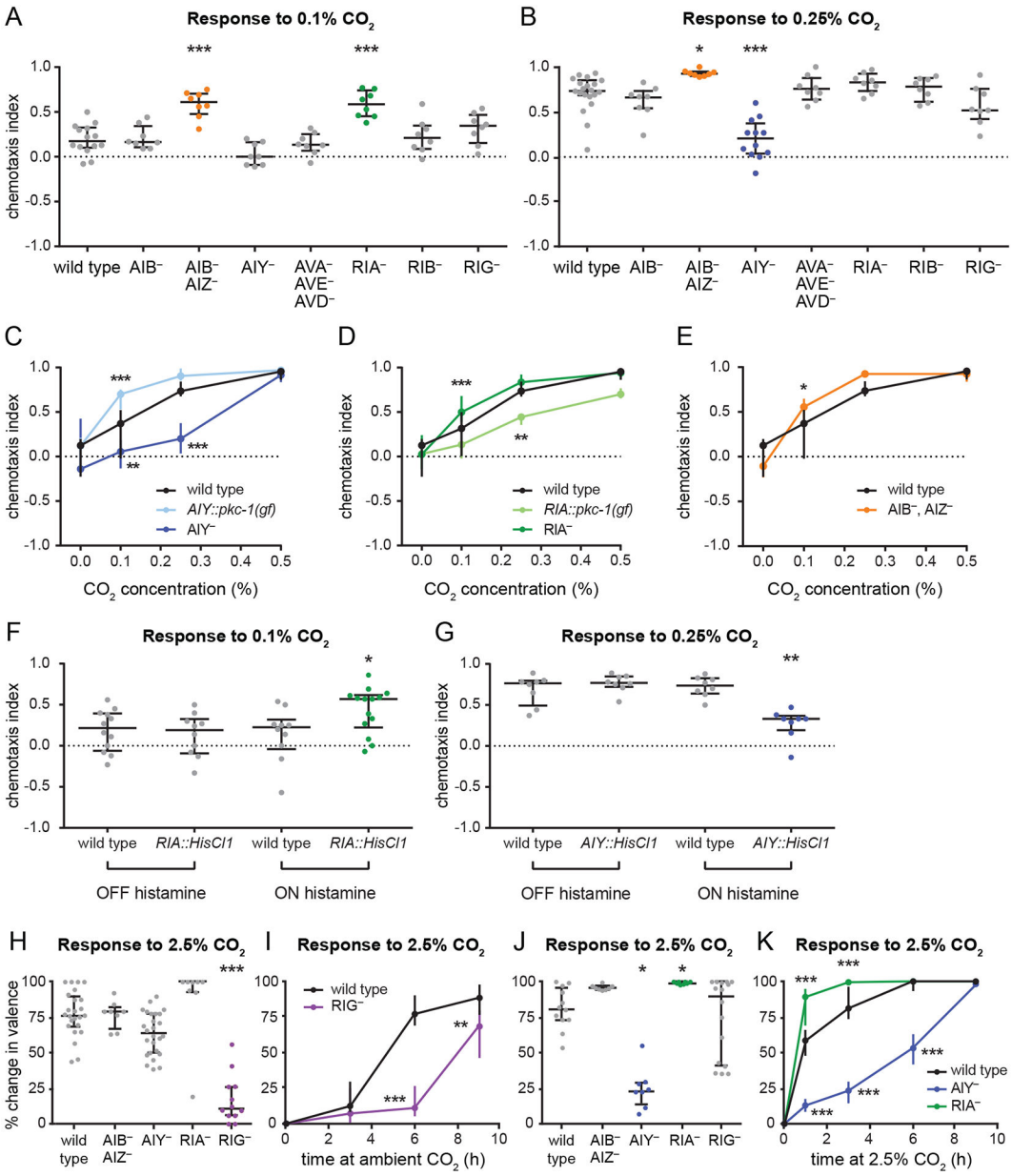

Figure 3. The same set of interneurons contributes to CO2 avoidance and attraction.

(A-B) In animals raised at high (2.5%) CO_2, silencing of AIZ and ablation of RIA enhances CO_2 attraction, while ablation of AIY reduces CO_2 attraction. Graphs show responses to 0.1% CO_2 (A) or 0.25% CO_2 (B). *p<0.05, ***p<0.001, one-way ANOVA with Dunnett's post-test (A) or Kruskal-Wallis test with Dunn's post-test (B). n=6–20 trials per genotype and condition.

(C) Ablation of AIY reduces CO_2 attraction. By contrast, animals with more active AIY neurons due to AIY-specific expression of *pkc-1(gf)* show enhanced CO_2 attraction. Animals were raised at high (2.5%) CO_2. **p<0.01, ***p<0.001, two-way ANOVA with Dunnett's post-test. n=6–20 trials per genotype and condition.

(D) Ablation of RIA enhances CO_2 attraction. By contrast, animals with more active RIA neurons due to RIA-specific expression of *pkc-1(gf)* show reduced CO_2 attraction. Animals were raised at high (2.5%) CO_2. **p<0.01, ***p<0.001, two-way ANOVA with Dunnett's post-test. n=8–24 trials per genotype and condition.

(E) Silencing of AIZ enhances CO_2 attraction. Animals were raised at high (2.5%) CO_2. *p<0.05, two-way ANOVA with Sidak's post-test. n=8–20 trials per genotype and condition.

(F-G) Animals with RIA neurons transiently silenced by expression of the histamine-gated chloride channel HisCl1 in RIA show enhanced CO_2 attraction (F). By contrast, animals with AIY neurons transiently silenced using the same approach show reduced CO2 attraction (G). Responses to 0.1% CO_2 (F) and 0.25% CO_2 (G) were tested for wild-type animals and animals expressing HisCl1 in either RIA or AIY without histamine (negative control) and with histamine (neuronal silencing); changes in CO_2 response were observed only in the presence of histamine. Animals were raised at high (2.5%) CO_2. *p<0.05, **p<0.01, one-way ANOVA with Sidak's post-test (F) or Kruskal-Wallis test with Dunn's post-test (G). n=8–14 trials per genotype and condition.

(H-I) Ablation of RIG delays the shift from CO_2 attraction to repulsion in animals raised at high (2.5%) CO_2 and transferred to ambient CO_2. Animals were tested for their response to 2.5% CO_2 after 3, 6, or 9 h at ambient CO_2. Responses were compared to those of animals of the same genotype raised at ambient CO_2 and high CO_2 to determine the percent change in valence (see Methods). Graphs show the percent change in valence after 6 h (H) or as a function of time (I). **p<0.01, ***p<0.001, Kruskal-Wallis test with Dunn's post-test (H) or two-way ANOVA with Sidak's post-test (I). n=8–26 trials per genotype, time point, and condition.

(J-K) Ablation of AIY delays the shift, and ablation of RIA accelerates the shift, from CO_2 repulsion to attraction in animals raised at ambient CO_2 and transferred to high (2.5%) CO_2. Animals were tested for their response to 2.5% CO_2 after 1, 3, 6, or 9 h at high CO_2. Responses were compared to those of animals of the same genotype raised at ambient CO_2 and high CO_2 to determine the percent change in valence (see Methods). Graphs show the percent change in valence after 3 h

(J) or as a function of time (K). *p<0.05, ***p<0.001, Kruskal-Wallis test with Dunn's post-test (J) or two-way ANOVA with Dunnett's post-test (K). n=8–16 trials per genotype, time point, and condition.

For A-K, graphs show medians and interquartile ranges. See also Figure S3.

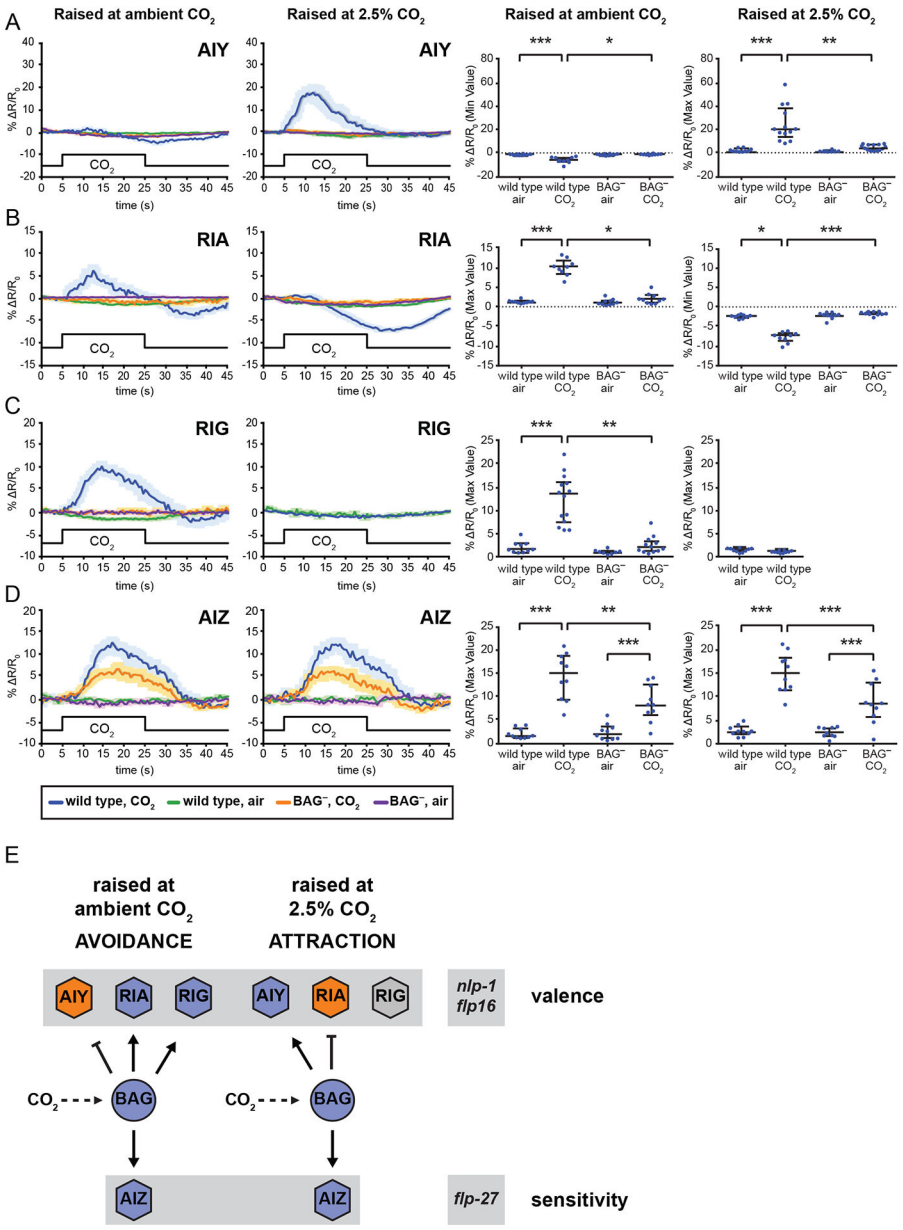

Figure 4. First-order interneurons contribute to CO_2 avoidance and attraction through experience-dependent modulation of their CO_2-evoked activity.

(A) AIY is inhibited by CO_2 in animals raised at ambient CO_2 and activated by CO_2 in animals raised at high (2.5%) CO_2. Both responses are BAG-dependent. *p<0.05, **p<0.01, ***p<0.001, Kruskal-Wallis test with Dunn's post-test. n=8–14 animals per genotype and condition.

(B) RIA is activated by CO_2 in animals raised at ambient CO_2, and inhibited by CO_2 in animals raised at high (2.5%) CO_2. Both responses are BAG-dependent. *p<0.05, ***p<0.001, Kruskal-Wallis test with Dunn's post-test. n=9–10 animals per genotype and condition.

(C) RIG is activated by CO_2 in animals raised at ambient CO_2, but does not respond to CO_2 in animals raised at high (2.5%) CO_2. The response is BAG-dependent. **p<0.01,

***p<0.001, Kruskal-Wallis test with Dunn's post-test (raised at ambient CO_2) or p=0.1060, unpaired t test (raised at high CO_2). n=8–14 animals per genotype and condition.
(D) AIZ is activated by CO_2 exposure in animals raised at both ambient and high (2.5%) CO_2. Both responses show BAG-dependent and BAG-independent components. **p<0.01, ***p<0.001, one-way ANOVA with Sidak's post-test. n=10 animals per genotype and condition.
For A-D, calcium responses were measured using the ratiometric calcium indicators yellow cameleon YC3.60 or YC2.12. Left graphs show composite calcium responses to a 20-s pulse of 15% CO_2. Solid lines indicate average calcium responses; shading represents SEM. Blue lines indicate the response of wild-type animals to CO_2; green lines indicate the response of wild-type animals to an air control; orange lines indicate the response of BAG-ablated animals to CO_2; purple lines indicate the response of BAG-ablated animals to an air control. Right graphs show maximum values (for excitatory or neutral responses) or minimum values (for inhibitory responses) of % ΔR/R0 for each animal. Lines show medians and interquartile ranges.
(E) A model for CO_2 response in *C. elegans.* Animals raised at ambient CO_2 avoid CO_2, while animals raised at high CO_2 (2.5% CO_2) are attracted to CO_2. CO_2 response valence is determined by the coordinated activity of three interneuron pairs postsynaptic to the CO_2-sensing BAG neurons: AIY, RIA, and RIG. In animals raised at ambient CO_2, activation of RIG and RIA combined with inhibition of AIY results in CO_2 avoidance. In animals raised at high CO_2, activation of AIY, inhibition of RIA, and silencing of RIG results in CO_2 attraction. Activation of a fourth interneuron pair, AIZ, dampens behavioral sensitivity to CO_2 regardless of valence. CO_2 response is regulated by a combinatorial code of neuropeptides: NLP-1 reduces CO_2 avoidance in animals raised at ambient CO_2, FLP-16 reduces CO_2 attraction in animals raised at high CO_2, and FLP-27 enhances CO_2 response under both conditions.
See also Figures S3 and S4.